Design for the lattice with 4-DBA structure of the compact laser-electron storage ring*

YANG Dan-Dan(杨丹丹)[1)] HUANG Wen-Hui(黄文会)

[1] Accelerator Laboratory Department of Engineering Physics, Tsinghua University, Beijing 100084，China
[2] Key Laboratory of Particle and Radiation Imaging of Ministry of Education, Tsinghua University, Beijing 100084, China

Abstract: We try to design the lattice with 2 super periods and 4-DBA structure in order to provide more drifts for the future development of the TTX source. Due to the space limitation in the lab, the 4-DBA lattice is suitable.In the paper,we present the lattice design with a 4-DBA structure mainly for the pulse mode of the compact laser-electron storage ring (LESR). Element parameters of the lattice are optimized with the help of the professional software and beam dynamics such as intra-beam scattering (IBS) and Compton scattering (CS) are calculated. Besides, the fringe field effect is analyzed with the numerical method.

Key words: lattice design, DBA, beam dynamics, scattered photon yield, fringe field

PACS: 41.60.-m, 29.27.Bd, 29.20.D- **DOI:** 10.1088/1674-1137/35/8/016

1 Introduction

The laser-electron storage ring (LESR), where the electron stored in a storage ring interacts repetitively with the laser pulse stored in an optical cavity, was first proposed by Z. Huang and Ruth in 1998 [1] for the purpose of increasing the collision frequency. Because of its compactness, low cost and high scattered photon energy, it provides a competitive and promising method for X-ray source.

The 2-DBA (Double Bending Achromat) racetrack lattice has been designed as one of our options for the Tsinghua Thomson X-ray source (TTX) and the dynamics in the lattice has also been calculated [2–4]. In order to obtain more drift sections to improve the flexibility for the future development, we try to design the new lattice which provides enough space for new experiment devices in the future. We have attempted the lattice designs of 2 super periods with 4-DBA and 6-DBA structures respectively, where the 6-DBA structure has more free-dispersion drifts. Due to the space limitation in the lab, the 4-DBA structure is more suitable for us. So the 4-DBA lattice is considered as another option for the TTX facility.

In this paper, we propose the lattice with 4-DBA structure for the pulse mode of the TTX source. We also present the optics and the parameters of the lattice with the help of professional softwares. The beam dynamics including IBS and CS is also discussed.

2 Lattice design for the TTX facility

2.1 Layout of the storage ring

The lattice is presented in Fig. 1. The lattice is similar to the Thom-X ring in France [5, 6]. One of the benefits of this design is that the interaction point (IP) is placed in the short dispersion-free straight section so that the optical cavity which can be located in between the gap of the adjacent dipoles is much shorter in the straight sections based on our needs. Fig. 2 shows the 3D layout of TTX facility and the lattice is also included. Beside other experiment-platforms in the lab, the left space for the storage ring is about 5 m×10 m. The lattice area without the transfer line and the optical cavity is about 3.7 m×6 m. We need to place the lattice in an appropriate position so that there is enough room for

Received 4 November 2010

* Supported by National Natural Science Foundation of China (10735050) and National Basic Research Program of China (973 Program)(2007CB815102)

1) E-mail: ydd08@mails.tsinghua.edu.cn

the transfer line, the optical cavity and the operation platform for the scattered x-ray.

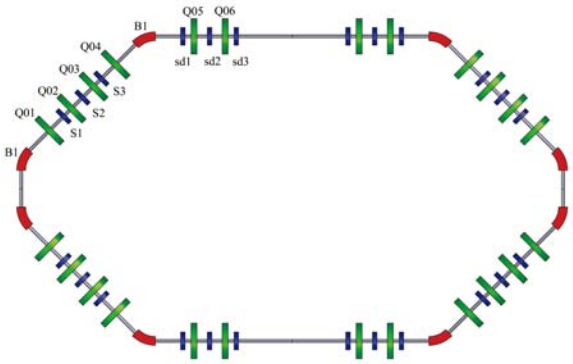

Fig. 1. Layout of the 4-DBA lattice (3.7 m×6 m).

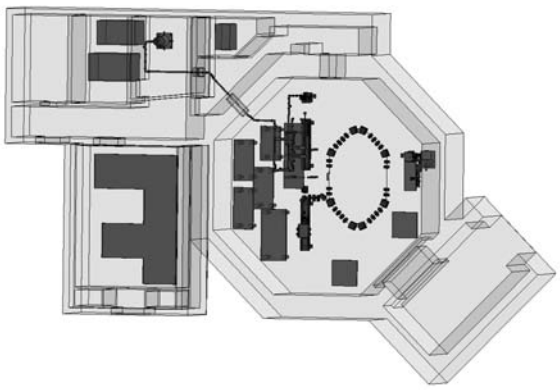

Fig. 2. The 3D layout of the TTX facility. We can see the position of the storage ring. The devices such as the optical cavity and the X-ray operation platform of the lattice are not drawn here.

The circumference of the ring is 15.12 m in order to match the optical cavity whose length is designed to be 3.78 m so that the electron and laser could interact at IP repetitively. There are 8 dipoles, 24 quadrupoles and 24 sextupoles in the lattice. The bending radius is 0.395 m while the bending angle is 45°. Groups of sextupoles are placed in the arc area to correct the natural chromaticity to zero while others are placed in the dispersion-free sections to enlarge the dynamic aperture (DA). The twiss parameters are plotted in Fig. 3 by the software MAD8 [7]. The beta function at IP is (0.129 m, 0.087 m) and it can be reduced by adjusting the quadrupole strength in order to enhance the yield of the scattered photon. The maximum length of the dispersion-free drifts is 1.4 m that is used to place the injection system and RF cavity. The maximum absolute strength of the quadrupoles is about 24/m^2 which is equal to 4 T/m with the electron energy of 50 MeV and it leaves room to improve the electron energy in the lattice. Parameters of the lattice are listed in Table 1. Natural chromaticity is calculated by OPA [8]. The momentum compaction factor is small enough for the pulse mode.

Table 1. Parameters of the lattice.

parameters	value
circumference/m	15.12
tunes	
horizontal	3.0836
vertical	1.6148
beta function at IP	
horizontal/m	0.129
vertical/m	0.087
maximal value of beta and dispersion	
horizontal/m	9.3651
vertical/m	8.0010
dispersion/m	0.8309
energy loss per turn	
synchrotron radiation/eV	1.401
compton scattering(laser energy 1 mJ)/eV	3.322
RF voltage/kV	300
RF frequency/MHz	992
harmonic number	50
momentum compaction factor	0.0165
energy acceptance	0.068
natural chromaticity	
horizontal	−9.744
vertical	−5.748

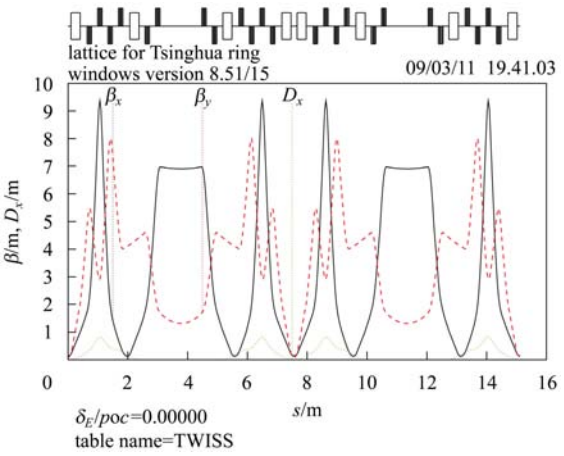

Fig. 3. Twiss parameters of the lattice for the pulse mode by the software MAD8 [7].

2.2 Dynamic aperture(DA)

We use the harmonic sextupoles placed in the dispersion-free area to enlarge the DA with the help of the software OPA [8]. We track the particles for 20000 turns without any errors in the position of IP and the maximum beta function (around Q2) respectively by OPA as shown in Fig. 4. The initial RMS transverse beam size at IP is 0.051 mm and after 400000 turns

it becomes 0.126 mm. The RMS beam size at the position of the maximal beta function is 0.433 mm and 1.074 mm after 400000 turns. The DA is large enough for the pulse mode concluded from the OPA result (Fig. 4). For DA optimization, besides the software OPA, we can also use the FMA method that has the advantage of checking the influence of the nonlinear effect only by tracking particles for limited turns. Because the OPA can only track the particles for finite turns, the real DA couldn't be known from its result while the FMA method could give more information about the DA. In order to check the nonlinear effect, we calculate the on-momentum frequency map [9] for 10000 turns as illustrated in Fig. 5. The tune shift with the momentum derivation is also included. The working point is between the 5th order-resonance

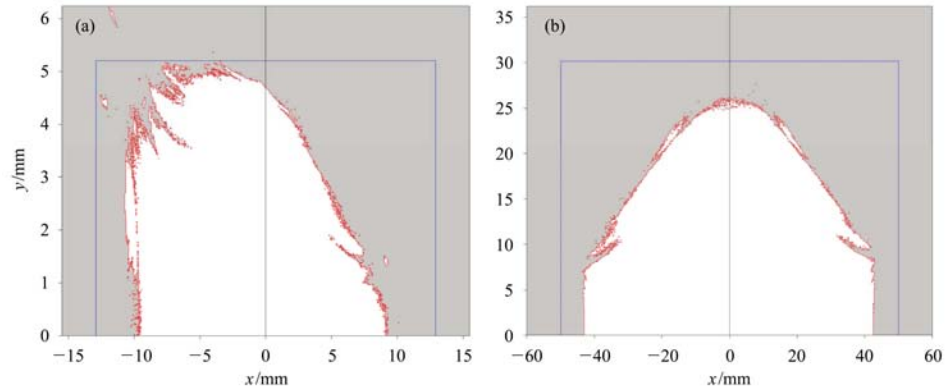

Fig. 4. The DA simulation for the position of (a) IP and (b) The maximal beta function with the help of the OPA. DA is more than 10 times the transverse beam sizes in both positions after 400000 turns respectively. So DA is large enough for the pulse mode. Because it could only track particles for limited turns, the real DA couldn't be known from the OPA result.

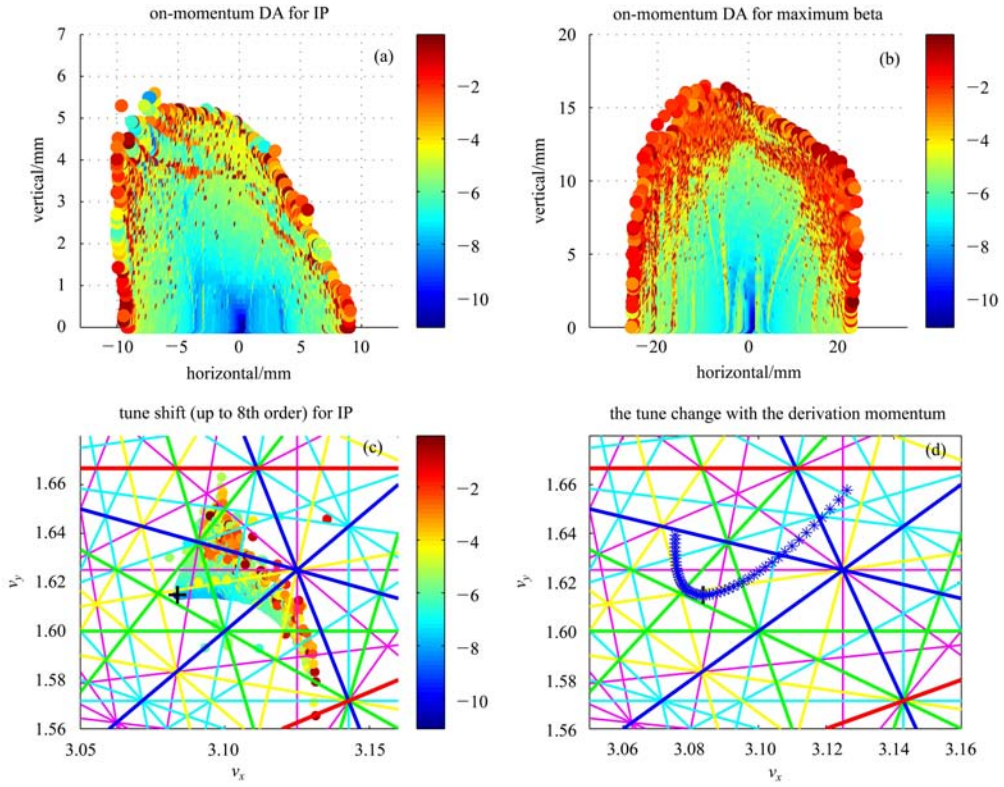

Fig. 5. (color online) (a)–(b)On-momentum DA for IP and maximum beta function; (c) The on-momentum frequency map; (d) The tune changes with the momentum derivation in the range of (−3%, 3%). The FMP method could give us more information about the real DA. The high-order resonance may affect the stability of the particles and limit the dynamic aperture to smaller size compared with the OPA results.

$2\nu_x + 3\nu_y - 11 = 0$ and the 6th order-resonance $\nu_x - 5\nu_y + 5 = 0$. From the FMA results, if the nonlinear effect is prominent,the particles may be lost at $x = \pm 6$ mm for IP while lost at $x = \pm 12$ mm for the maximum beta respectively although they can survive in the OPA tracking. Although the DA is smaller than the OPA results, it's still large enough for the pulse mode. The shift compared with the on-momentum tune value (3.0836, 1.6148) is below 2% which is acceptable for us.

3 Beam dynamics and the simulation result

The main beam dynamics in the compact storage ring includes the intra-beam scattering (IBS), the Compton scattering (CS) and synchrotron radiation (SR). Because of the low electron energy and the compactness of the storage ring, the most important factor is IBS that is dominant in the transverse dynamics. Besides, CS will cause a large energy spread, so it works with IBS together in the longitudinal dynamics.

Parameters for the electron beam and laser pulse in the simulation are shown in Table 2. Because the ratio of longitudinal beam size and spread energy keeps constant in the storage ring, the initial value of energy spread in the simulation matches with the pulse length of 10 ps to avoid filamentation in the longitudinal phase space.

Table 2. Parameters for the electron beam and laser pulse.

parameters	value
electron	
energy/MeV	50
beam charge/nC	1.0
initial RMS transverse emittance/nm·rad	20
initial energy spread	0.2121%
beam pulse length/ps	10
laser	
pulse energy/mJ	1.0
laser photon wavelength/nm	800
rayleigh length/mm	6
transverse size at IP/μm	20
pulse length/fs	100
collision angle/(°)	178

3.1 Beam dynamics

The effect of synchrotron radiation (SR) is not strong in such compact storage ring compared with IBS and CS because of the low electron energy. The energy loss per turn is $U_{\rm SR} = 1.401$ eV. The critical energy of the radiated photon is $u_{\rm c} = 0.702$ eV. The number of photons radiated per turn because of SR is $\overline{N} = 6.48$.

CS will cool down the transverse dynamics [10]. So the laser cooling effect of CS could decrease the transverse emittance growth caused by IBS. As the laser energy increases, the cooling effect of CS becomes stronger. However, the IBS still plays a more important role in the horizontal emittance. For the longitudinal dynamics, the CS will contribute to the energy spread [9]. Take CS alone into account, we can calculate the equilibrium transverse emittance and energy spread. With the damping time together, the influence of CS in the transverse and longitudinal dynamics can be measured by the three parameters simply.

The influence of IBS is very strong in the low energy range. The horizontal emittance increases rapidly due to IBS.The simulation of IBS is based on the macroparticles algorithm and the binary collision model is described in detail in Ref. [11].

Besides, the scatter photon yield is also calculated by the expression as follows [12]:

$$n_x = C_{\rm off}\frac{n_{\rm e}n_{\rm l}\Sigma}{\sqrt{2}\pi}\frac{1}{\sqrt{(\sigma_{ey}^2+\sigma_{\rm ly}^2)[(1-\cos\alpha)(\sigma_{ex}^2+\sigma_{\rm lx}^2)+(1+\cos\alpha)(\sigma_{ez}^2+\sigma_{\rm lz}^2)]}}, \quad (1)$$

where Σ is the Compton scattering cross-section; $n_{\rm e}$ and $n_{\rm l}$ are the numbers of electrons and laser photons respectively; σ_{ex}, $\sigma_{\rm lx}$, σ_{ey}, $\sigma_{\rm ly}$, σ_{ez} and $\sigma_{\rm lz}$ are the RMS transverse and longitudinal sizes of electron beam and laser pulse; $C_{\rm off}$ is the coefficient for the decrease of the scattered photons caused by system errors and in the ideal condition, $C_{\rm off} = 1$; α is the collision angle and for the head-on collision, $\alpha = \pi$. For non-head-on collision, the scattered photon yield n_x depends on the the longitudinal sizes. Because the longitudinal beam size σ_{ez} is proportional to the energy spread, the influence of CS on the spread energy will be considered when the scattered photon yield is calculated.

3.2 The simulation result

The injection frequency of the electron is 50 Hz for the lattice. The life of the electron beam is about 20 ms and we track the particles for about 400000 turns corresponding to 20.16 ms. The simulation

results including the transverse emittance, the relative energy spread and the yield of the scattered photon with the laser energy of 1 mJ are shown in Fig. 6. The horizontal emittance growth caused by IBS is about a factor of 6. Here the influence of CS and SR is ignored because it's relatively small compared with IBS, but for the longitudinal phase space, the IBS and CS are considered together while the SR almost has nothing to do with the longitudinal dynamics. It shows that the relative energy spread has about 2-time growth and the scattered photon yield decreases by 50% compared with the initial yield owing to the strong IBS effect. The scattered photon yield is related with the transverse emittance and enrgy spread, so the yield can be enhanced by optimizing the lattice to suppress the IBS effect.

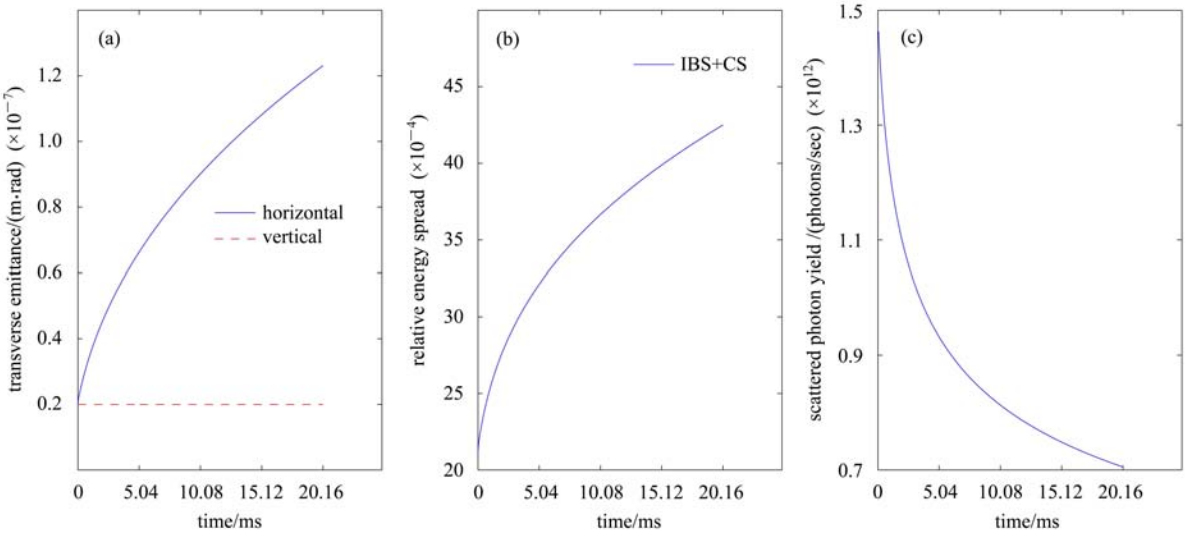

Fig. 6. (a) The transverse emittance caused by IBS; (b) The relative energy spread by IBS and CS together; (c) The yield of the scattered photon. It's shown that the horizontal emittance has a 6-time growth while the energy spread is increased by 2 times. The scattered photon yield drops to about 50% of the value at the starup. All simulations are carried out with the laser pulse energy of 1 mJ.

4 Fringe field effect of the quadrupoles

In this section, the fringe field effect of magnets is studied for the compact lattice. The development of theoretical analytical techniques such as Li algebra and differential algebra makes the simulation and calculation in fringe field effect feasible and convenient. As we know, during the design of the large storage ring where the fringe field extensions are much smaller than the magnet length, the fringe field effect is always ignored and the traditional hard-edge model is used as the approximate treatment. For the compact storage ring, the fringe field effect becomes non-negligible for particle motion and beam dynamics because of the specific characteristics of a small ring lattice such as the large bend angle and the comparability between the magnet aperture and the steel length [13]. There are many articles that provide analytical methods for the fringe field effect [14–17]. In this section, we apply the fringe field theory to the single Q01–Q06 based on the focusing function $k(z)$ from the field data obtained in the magnet simulation.

4.1 Transfer matrix with the fringe field

With the magnetic field data from the simulation, we can obtain the focusing function of the quadrupoles $k(z)$, which includes the fringe field distribution. The value of $k(z)$ changes with the longitudinal position z, so the motion equations can be expressed as follows:

$$x'' + k(z)x = 0, \tag{2}$$

$$y'' - k(z)y = 0. \tag{3}$$

For the focusing magnet, Formula (2) represents the particle motion for x direction while (3) for y direction. The equations can be solved numerically by the slice method or Runge-Kutta algorithm. In the slice method, it divides the field into slices and each slice can be dealt with the hard-edge model while in the Runge-Kutta algorithm, it decomposes the motion Eqs. (2) and (3) into two first-order differential equations and obtains the solutions of the motion

equations. Then we can obtain the transfer matrices of the quadrupoles that contain the fringe field effect. Take the quadrupole Q02 (shown in Fig. 1) for example. The matric elements of Q02 for x motion and y motion respectively are illustrated in Fig. 7. Because of the symmetry for the field distribution, the diagonal elements should be the same. The transfer matrix M_x is:

$$M_x = \begin{bmatrix} 0.14277 & 0.29946 \\ -3.27126 & 0.14277 \end{bmatrix}, \tag{4}$$

while the transfer matrix M_y:

$$M_y = \begin{bmatrix} 2.00700 & 0.76475 \\ 3.95952 & 2.00700 \end{bmatrix} \tag{5}$$

and the determinant of M_x and M_y is equal to unity and the results are reasonable for the symmetry field distribution. The results obtained from the slice method and Runge-Kutta algorithm are almost the same.

4.2 The quadrupole parameters

With the method introduced in 4.1, the transfer matrices of the quadrupoles can be obtained. For the symmetric field distribution, there are only two independent parameters in the transfer matrices and it's the same for the hard edge model. So it's possible to define the equivalent hard edge model, which can be expressed as the product of three matrices [14]:

$$M = DHD, \tag{6}$$

M is the transfer matrix with the fringe field obtained in 4.1; D is the transfer matrix of the drift with the distance $l-L/2$, where l is the distance from the center to the entrance or exit of the magnet, given as:

$$D = \begin{bmatrix} 1 & l-L/2 \\ 0 & 1 \end{bmatrix}, \tag{7}$$

H is the tansfer matrix for a hard edge model with the form as:

$$H = \begin{bmatrix} \cos(\sqrt{K}L) & \sin(\sqrt{K}L)/(\sqrt{K}) \\ -\sqrt{K}\sin(\sqrt{K}L) & \cos(\sqrt{K}L) \end{bmatrix}. \tag{8}$$

There are two independent equations from (6)–(8) and they could be solved numerically to obtain the parameters K and L. For the quadrupole Q02, the parameters for the traditional and equivalent hard edge models respectively are listed in Table 3, where the subscripts of F and D stand for the focusing and defocusing directions. It shows clearly the differences between these two hard edge models. Besides,the parameters K and L for the focusing and defocusing directions respectively in the equivalent models are not the same because of the fringe field effect. In order to apply the lattice design code as MAD and AT, we use the mean values of K and L in the focusing and defocusing models as an approximate treatment. The parameters in the equivalent model are different from the traditional model and the magnets should be redesigned to make the parameters in the equivalent models coincident with the traditional model as in Table 3.

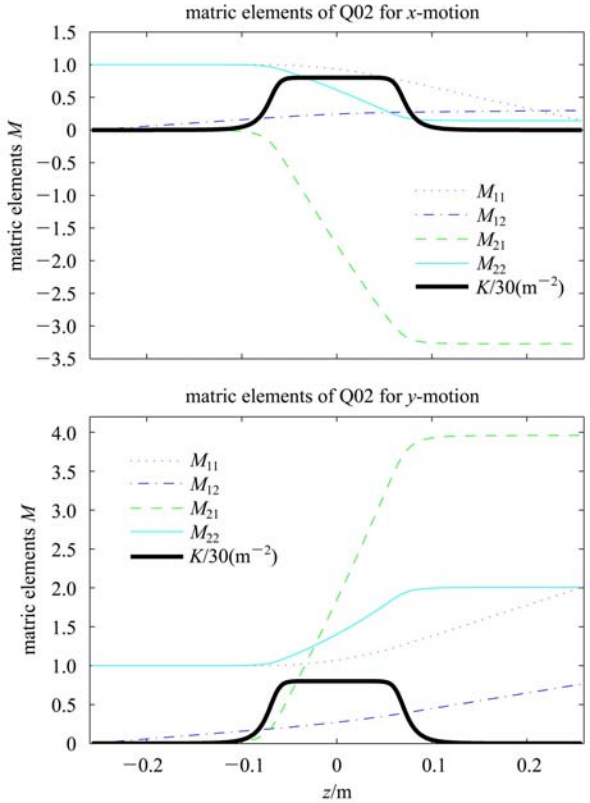

Fig. 7. The matric elements of Q02 for x-motion and y-motion respectively. The filed region in the simulation is cut off at the positions of $z = \pm 0.258$ m beyond which the magnetic field is very small and can be neglected.

Table 3. Parameters of Q02 for two hard edge models.

parameters	value
traditional model	
K, m^{-2}	24.03313
L, m	0.15
equivalent model	
K_F/K_D, m^{-2}	22.5909/22.4403
L_F/L_D, m	0.159705/0.160523

4.3 The method for the field interference

We take the quadrupole doublet as Q01 and Q02 for example. The distance between Q01 and Q02 is

0.2 m and the field interference effect exists in the region between these two magnets. In order to obtain the parameters of the hard-edge models used in the simulations, the quadrupole centers remains in the same position and they are separated at z_0 where the focusing function $k(z)$ equals to 0. Because of the field interference effect, the field distribution of the magnets becomes asymmetric. The transfer matrix of Q02 is defined as:

$$M = D_2 H D_1, \tag{9}$$

where D_1 and D_2 are the transfer matrices of the drift with the length of $l - L_1$ and $l - L_2$ respectively; the parameters L in the transfer matrix H is defined as:

$$L = L_1 + L_2. \tag{10}$$

Table 4. Parameters of Q02 in equivalent model with fringe interference

parameters	value
$K_{\rm F}/K_{\rm D}$, $\rm m^{-2}$	22.9732/22.824
$L_{1\rm F}/L_{1\rm D}$, m	0.079504/0.079881
$L_{2\rm F}/L_{2\rm D}$, m	0.079603/0.080040

The transfer matrices M_x and M_y are as :

$$M_x = \begin{bmatrix} 0.132434 & 0.286357 \\ -3.311069 & 0.391533 \end{bmatrix}, \tag{11}$$

$$M_y = \begin{bmatrix} 2.020864 & 0.609950 \\ 4.015645 & 1.706866 \end{bmatrix}. \tag{12}$$

The diagonal elements are not equal to each other because of the field interference. The parameters K, L_1 and L_2 can be solved with the numerical method. The results are listed in Table 4. It shows that L_1 and L_2 are a little different and not equal to $L/2$ due to the asymmetry of the field distribution. The difference of L_1 and L_2 will become larger if these two magnets are closer to each other.

5 Summary

The lattice with 4-DBA structure for the pulse mode is presented in this paper. Based on the designed lattice, we calculate the DA at the position of IP and the maximal beta function and also the on-momentum frequency map. It's obvious that DA is large enough for the pulse mode. It's known that the IBS dominates in the transverse dynamics while the IBS and CS contribute to the longitudinal dynamics together. The SR effect is relatively small because of the low electron energy. Besides, the CS effect will become stronger when the laser energy grows. The yield of the scattered photon is also calculated.It drops to 50% of the value at the starup. So the IBS suppression is very important to increase the yield of the scattered photon and beam stability. Besides,the fringe field effect in the single quadrupole and the field interference are preliminarily analyzed with numerical methods. Two hard-edge models as traditional and equivalent models are established and the parameters in these models are obtained.The field data in the simulation are obtained with the magnet software. In the future,the magnet models will be designed for a better field distribution.

The authors are greatly indebted to Yu Peicheng for the helpful instructions and discussions on lattice design and the IBS simulation.

References

1 HUANG Z, Ruth R D. Phys. Rev. Lett., 1998, **80**: 976
2 YU Pei-Cheng et al. Phys. Rev. ST Accel Beams, 2009, **12**: 061301
3 YU Pei-Cheng, HUANG Wen-Hui. Nucl. Instrum. Methods A, 2008, **592**: 1
4 YU Pei-Cheng et al. Chin. Phys. C (HEP & NP), 2009, **33**(S2): 151
5 Bruni C et al. A Compact Ring for Thom-X Ray Source, in Proceeding of PAC-09
6 Variola A et al. THOMX Conceptual Design Report
7 MAD8,http://project-madwindows.web.cern.ch/project-madwindows/MAD-8
8 OPA lattice design code, http://slsbd.psi.ch/ streun/opa/
9 Nadolski L, Laskar J. Phys. Rev. ST Accel Beams, 2003, **6**: 114801
10 Bulyak E, Skomorokhov V. In Proceeding of E-PAC, 2004 http://accelconf.web.cern.ch/Accel Conf/e04/papers/weplt138.pdf
11 Sergei Nagaitsev. Phys. Rev. ST Accel Beams, 2005, **8**: 064403
12 HUANG Wen-Hui, HE Xiao-Zhong et al. HEP & NP, 2004, **28**(4): 446–450 (in Chinese)
13 Wilson JE J N. Small Ring Lattice Problems, CERN Accelerator School, CERN 95-06, 1995
14 Lee-Whiting G E. Nucl. Instrum. Methods, 1969, **76**: 305
15 Irwin J, WANG C X. Explicit Soft Fringe Maps of a Quadrupole, PAC95
16 WANG J G. Magnetic Fringe Fields and Interference in High Intensity Accelerators, Nova Science Publishers, 2009
17 Steffen K G. High Energy Beam Optics, 1965